Computer Assisted Methods in Engineering and Science
30(1): 41–54, 2023, doi: 10.24423/cames.455

This article belongs to the *Special Issue on Information Theory with Artificial Intelligence in 5G/6G Networks* edited by Dr. A.K. Budati, Dr. M.K. Hasan, Dr. R. Arthi, Dr. K. Thangavel

Hybrid Texture and Gradient Modeling for Dynamic Background Subtraction Identification System in Tobacco Plant Using 5G Data Service

M.T. THIRTHE GOWDA[1),2)*], J. CHANDRIKA[3)]

[1)] *Department of Computer Science and Engineering, Government Engineering College, Hassan, Karnataka, India*

[2)] *Department of Computer Science and Engineering, Malnad College of Engineering, Hassan, Karnataka, India*

[3)] *Department of Information Science and Engineering, Malnad College of Engineering, Hassan, Karnataka, India; e-mail: jc@mcehassan.ac.in*

[*] *Corresponding Author e-mail: thirthegowda.gech@gmail.com*

Background: Detecting the plants as objects of interest in any vision-based input sequence is highly complex due to nonlinear background objects such as rocks, shadows, etc. Therefore, it is a difficult task and an emerging one with the development of precision agriculture systems. The nonlinear variations of pixel intensity with illumination and other causes such as blurs and poor video quality also make the object detection task challenging. To detect the object of interest, background subtraction (BS) is widely used in many plant disease identification systems, and its detection rate largely depends on the number of features used to suppress and isolate the foreground region and its sensitivity toward image nonlinearity.
Methodology: A hybrid invariant texture and color gradient-based approach is proposed to model the background for dynamic BS, and its performance is validated by various real-time video captures covering different kinds of complex backgrounds and various illumination changes. Based on the experimental results, a simple multimodal feature attribute, which includes several invariant texture measures and color attributes, yields finite precision accuracy compared with other state-of-art detection methods. Experimental evaluation of two datasets shows that the new model achieves superior performance over existing results in spectral-domain disease identification model.
5G assistance: After successful identification of tobacco plant and its analysis, the final results are stored in a cloud-assisted server as a database that allows all kinds of 5G services such as IoT and edge computing terminals for data access with valid authentication for detailed analysis and references.

Keywords: background subtraction (BS), local binary pattern (LBP), tobacco plant, texture, Gaussian mixture model (GMM), illumination changes, plant disease identification system.

1. Introduction

In agriculture, plant diseases have always been a primary concern since they affect overall crop yields and quality. The symptoms are identified based on minor to severe damage of plant leaves and impact heavily on the planted crops. In order to prevent agricultural economy losses, various methodologies are established to detect the disease. However, precise identification of plant diseases requires the most appropriate analysis and decision-making process. Moreover, it is essential to process large amount of data to get superior results in detecting plant disease. Currently available sample image processing-based models do not contain enough information for improved decisions. A comprehensive dataset must contain a video sequence.

Progression in vision analyses and the significant advancement in artificial intelligence offer new solutions to precision agriculture. However, when examining the large sets of crops, one of the major challenges in the automatic detection of any plant disease based on the symptoms and shape variations of the plant leaf is the vision analysis that includes moving object detection and segmentation. The process of segmenting a moving object into a foreground region (plant region) and background scenes (static region) is called the BS process. The two most commonly used techniques for BS are statistical parametric and nonparametric-based techniques. In the parametric approach, by modeling the pixel intensity changes, one can identify the background using some normal distribution [1]. In nonparametric-based approach, the background model is estimated based on pixel intensity variance independently [2] for each incoming frame. This latter approach is able to detect the targets with higher sensitivity and also to adapt faster to changes in the background process. It has metrics of low complexity since simple modeling techniques are used for accurate background estimation. However, the metrics suffer from accuracy loss caused by background changes, which leads to some uncertainty in accurate estimation.

In recent years, texture models have gained momentum in vision applications for high accuracy image tasks.

2. Related works

Plant disease identification based on real-time visual inspection is a difficult task to accomplish on a regular basis over large field area, and it is also time-consuming and expensive. To mitigate this problem, several research works introduced vision-based automated models with improved detection accuracy. Classical vision applications require the most effective foreground separation for analyzing the object of interest. The complex background is another issue while studying the real-time captured dataset in an open outdoor environment. In ad-

dition to this, computational complexity and memory space requirements of various existing vision-based processing models are not applicable for vision-based plant disease identification systems.

Many of the previous works were devoted only to one or more invariant models that are less sensitive to any moving foreground object as proposed by [3] or appropriate quantitative evaluation to estimate motion events [4]. To reduce the cost of complex arithmetic, simple texture models were investigated in previous works. In [5], a LBP and CLBP approach with sign and magnitude components was employed for texture classification. An image local texture features were extracted by using CLBP_C, CLPB_S and CLPB_M. In [6] codebook algorithm was used based on edges and texture analysis to verify foreground pixels. In some cases, edge and spatial intensity measures were used to explore the color information and its discriminations with the background. In [7], spatial-color binary patterns were used to model the dynamic backgrounds.

Texture models always show significant improvement in accuracy as compared to motion models. In [8], the authors reduced the impact of shadows by incorporating the intensity changes of one-pixel over-illumination changes using a photometric invariant model. However, for outdoor videos to reduce the variance and improve the accurate computation of dynamic events the multi-model approaches are always required.

To the best of our knowledge, all previous methodologies proposed for template-based approaches in dynamic background models have neglected the effect of variations caused by boundaries that occurred only in illuminated field site videos. Whereas, the multimodal approaches using motion events failed over blurred scenes. The main drawback of template-based dynamic BS is its complex arithmetic in comparison with the motion model counterparts. In [9], scale-invariant local texture patterns for appearance information and associated spatial exploration of objects of interest at each input sequence were developed. Andrushia and Patricia [10] introduced Gaussian mixture-based BS to detect and classify diseases in grape leaves. Multimodal features, including color, the gray level co-occurrence matrix (GLCM) texture and shape attributes, were extracted for disease abnormalities, Furthermore, an artificial bee colony model was used for feature sub-set evaluation to generate an optimal feature set.

Kumar *et al.* [11] proposed a Gaussian mixture model-based template generation to segment the plant leaves as foregrounds and used an artificial bee colony-based fuzzy C means model for the identification procedure. To improve the detection rate, a singular value decomposition (SVD) was incorporated to reduce the dimensions of multiple feature vectors used for final classification. In [12], the hyper spectral imaging and a wavelength selection strategy were used to identify and examine the virus-infected area in a tobacco plant. In [13], for dynamic background subtraction for every frame instant, a unified approach

color category analysis on categorical entropy was employed, although it is unreliable for shape and scale variations. In [14], the spatial temporal classification is modeled using the least number of temporal features with spatial features, and its sensitiveness toward dynamic background changes is also very low, which improves the detection rate significantly. In these cases, background model contains unique features to subtract background scenes. In [15], a spatiotemporal model was proposed to segment dynamic background and moving objects. However, the dynamic nature of outdoor videos causes large variance over different classes of background moving objects. In [16], the AI-based deep learning models used for object detection and localization of objects for 5G networks are presented. In [17], a Deep Neural Network (DNN)-based offline template model is used for the real-world 5G multi-access edge computing testbed to meet requirements such as improved detection accuracy with ultra-low latency for object detection. In [18], the 5G technology enabled intelligent video surveillance applications are used to detect human object detection by using cascaded object detection method.

3. Dynamic background model

In general, for improved object detection rate, the template models used for detecting the foreground should comprise more than one feature attribute for subtracting the background and foreground for plant detection, as shown in Fig. 1. The proposed plant detection frameworks include a hierarchical stage which includes: feature extraction, template modeling and BS, as shown in Fig. 2.

Fig. 1. Input sample frame from tobacco plant.

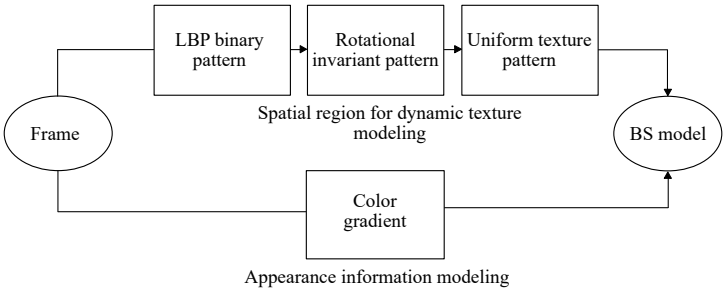

Fig. 2. Block diagram of the BS model.

Initially, a template is formulated by extracting feature attributes from incoming frames and forms the template used as reference model to isolate foreground regions. With the inclusion of multimodal feature attributes, the issues related to illumination changes and associated spatial variations are suppressed.

The motivation for the foreground detection (FD) technique is that the texture feature and the color feature details of a frame: mean, standard deviation and energy measures, as shown in Fig. 3, are also used to model the background. The FD technique is used to model the background using rotational invariant and uniform texture features. Along with this feature, color features are also used to handle the illumination changes (sudden/gradual). After modeling the pixels in the background, the frame differencing method is applied to segregate between the stationary and nonstationary pixels. Optimal number of features is used to model the background, which reduces the overall computational time and associated computational complexity, which can support a wide range of outdoor video types.

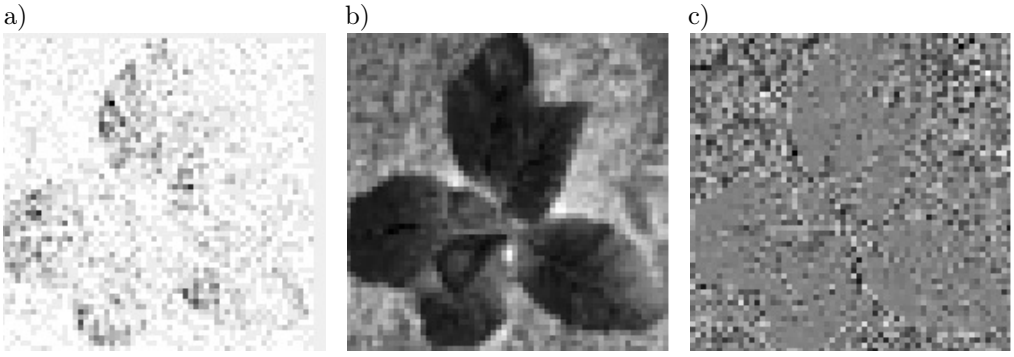

Fig. 3. Color attributes model: a) mean measure, b) ST measure, c) energy measure.

The above procedure for dynamic BS is summarized as follows:

Algorithm: Background subtraction

TL – threshold level,
CG – color gradient computation,
MB – macroblock,
CLBP – computation of local binary pattern,
CRIT – computation of rotational invariant texture,
CUT – computation of uniform texture,
SF – separated foreground.
FD (Input frame, foreground pixel)
//**Input** – Sequence of crop field video frames
//**Output** – Separated foreground (Plant region)

Step 1: set sigma as TL1 // variance value
set minimum number of transitions as TL2 // uniform texture margin value
set margin for invariant texture as TL3 // rotational texture margin value

Step 2: for $i \leftarrow 1$ to height of frame do
for $j \leftarrow 1$ to width of frame do
for $m = 1{:}3$
$P1(i,j) = CG(i,j,m)$
end
end
end
B = macroblock conversion (for each frame) // 3×3 matrix
$TM = CLBP(B)$;
$P2 = RITM(TM)$;
$P3 = CUT(TM)$;

Step 3: for $i \leftarrow 1$ to height of frame do
for $j \leftarrow 1$ to width of frame do
if $TL1(i,j) \leq P1(i,j)$ && $TL2(i,j) \leq P2(i,j)$ && $TL3(i,j) \leq P3(i,j)$ then
$SF(i,j) = 0$ // background region
else
$SF(i,j) = 1$ // foreground region
end
end
end.

The proposed system is tested for different datasets in terms of videos capturing tobacco plant and successfully stored using a cloud-assisted server for 5G services. Nkenyereye *et al.* [19] proposed a new protocol for a cloud-assisted video reporting service in 5G enabled networks. Furthermore, the hybrid method is used for modeling BS. For modeling the moving objects, an extended center symmetric local binary pattern (XCS-LBP) approach was developed. However, it has the limitation of poor sensitiveness toward dynamic background with various complex backgrounds, which reduces the detection rate. The object detection framework proposed in [20] used highly complex outdoor CCTV video sequences and introduced CNNs to accomplish the classification. In order to reduce the computational complexity and improve the convergence rate, an optimal BS model is used to isolate the object of interest from input video sequences.

3.1. Texture model

To reduce the sensitivity of the proposed BS process to different scale variations, the template is modeled by using highly discriminate texture features (rotational invariant and uniform) using local binary pattern (LBP), as shown in Fig. 4. Initially, LBP texture classification is done over each input macroblock of size 3×3 using successive swapping and sequential comparison. Based on true and false rates, texture patterns are obtained using hierarchical bit concatenation. In this study, the sliding widowing length is fixed for the entire texture classification process. Moreover, to explore the uniformity of extracted LBP patterns, the successive modulo-2 operation is carried and based on bit transition input, and LBP patterns are classified, which shows improved invariance to scale rotational changes at the input. The rotational and scale invariant patterns extracted from each incoming frame are successively used, and templates are updated periodically at regular time intervals for improved object detection rate.

3.1.1. GLCM feature extraction and relevant texture bound analysis. There are numerous ways to explore the spatial correlation level of the input object of interest, which includes the successive intensity of one pixel with its surroundings. In most cases, GLCM is widely used as the most predominant texture feature extraction in many image processing applications due to its inherent invariant characteristics. The texture analyses include the following three different statistical characteristics of the spatial relationship:

- orientation texture features (0°, 45°, 90°, 135°),
- texture displacement measurement,
- statistics texture features.

In this study, 20 GLCM feature attributes are used to explore the extract texture features, as shown in Table 1, to represent the visual perceptions of all three texture classified patterns of tobacco plants as given below:

$$\text{contrast} = \sum_{l,m=0}^{M-1} (X_{lm} - m)^2,$$

$$\text{correlation} = \sum_{l,m=0}^{n} X_{lm} \frac{(1-\mu)(m-\mu)}{\sigma^2},$$

$$\text{energy} = \sum_{l,m=0}^{M-1} (X_{lm})^2,$$

$$\text{homogeneity} = \sum_{l,m=0}^{M-1} \frac{X_{lm}}{1+(l-m)^2},$$

Table 1. Texture retention level analysis over different classifications using GLCM feature attributes.

LBP GLCM feature set	Autocorrelation: 5.495571161048689e+01 Contrast: 7.588576779026217e+00 Correlation: -1.368743615934625e-02 PeakCorrelation: -1.368743615934708e-02 Prominence: 3.408785528506035e+02 Shade: -4.187583229296714e+01 Dissimilarity: 1.084082397003745e+00 Energy: 7.163376888440012e-01 Entropy: 5.735740801632593e-01 Homogeneity: 8.644897003745319e-01 probability: 8.392322097378278e-01 Variance: 5.851847330729167e+01 sumaverage: 1.483333333333333e+01 sumvariance: 2.137973861250072e+02 sumentropy: 4.662271291664292e-01 Diffvariance: 7.588576779026217e+00 Diffentropy: 4.310625596314219e-01 infmeasurecorrelation: -3.412610510646425e-04 Diffnormalized: 9.277278401997503e-01 momentnormalized: 9.328444532829538e-01
Rotational invariant LBP GLCM feature set	Autocorrelation: 1.844631710362048e+00 Contrast: 5.141635455680400e+00 Correlation: -2.323301721585085e-02 PeakCorrelation: -2.323301721585064e-02 Prominence: 2.132153078330428e+02 Shade: 2.917455027845197e+01 Dissimilarity: 7.345193508114857e-01 Energy: 8.035305567634714e-01 Entropy: 4.211671546443120e-01 Homogeneity: 9.081850811485643e-01 probability: 8.933208489388265e-01 Variance: 4.360827590999532e+00 sumaverage: 2.758988764044944e+00 sumvariance: 1.071891292246085e+01 sumentropy: 3.484349634716172e-01 Diffvariance: 5.141635455680400e+00 Diffentropy: 3.357850513354065e-01 infmeasurecorrelation: -1.472612423420681e-03 Diffnormalized: 9.510320432792343e-01 momentnormalized: 9.544988012771646e-01
Uniform LBP GLCM feature set	Autocorrelation: 2.930084269662921e+01 Contrast: 2.247668539325843e+01 Correlation: 1.866771091344312e-02 PeakCorrelation: 1.866771091344362e-02 Prominence: 1.151444616762521e+03 Shade: -4.320951728935360e+01 Dissimilarity: 3.210955056179775e+00 Energy: 2.842720923907537e-01 Entropy: 1.320260095425698e+00 Homogeneity: 5.986306179775280e-01 probability: 3.982521847690387e-01 Variance: 4.039930293432038e+01 sumaverage: 1.078648564294632e+01 sumvariance: 1.190618977028714e+02 sumentropy: 1.002308924970338e+00 Diffvariance: 2.247668539325843e+01 Diffentropy: 6.897332129316787e-01 infmeasurecorrelation: -2.633887401935781e-04 Diffnormalized: 7.859363295880150e-01 momentnormalized: 8.010912797056776e-01

$$\text{entropy} = \sum_{l,m=0}^{M-1} -\ln(X_{lm})X_{lm},$$

$$\text{shade} = \text{sgn}(Q)|Q|^{1/3},$$

$$\text{prominence feature} = \text{sgn}(R)|R|^{1/3},$$

$$\text{autocorrelation} = \sum_{l,m=0}^{M-1} lm(X_{lm}),$$

$$\text{dissimilarity} = \sum_{l,m=0}^{M-1} |l-m|(X_{lm}),$$

$$\text{cluster shade} = \sum_{l,m=0}^{M-1} (l+m-\mu 1-\mu 2)^3(X_{lm}),$$

$$\text{cluster prominence} = \sum_{l,m=0}^{M-1} (l+m-\mu 1-\mu 2)^4(X_{lm}),$$

$$\text{maximum probability} = \max\{X_{lm}\}\,\forall l,m,$$

$$\text{inverse difference} = \sum_{l,m=0}^{M-1} \frac{C_{lm}}{1+(l-m)},$$

$$\text{inverse difference moment} = \sum_{l,m=0}^{M-1} \frac{C_{lm}}{1+(l-m)^2},$$

$$\text{sum of square} = \sum_{l,m=0}^{M-1} X_{lm}(l-\mu)^2,$$

$$\text{sum entropy} = -\sum_{l,m=0}^{M-1} X_{lm}\log(X_{lm}),$$

$$\text{inverse measure of correlation} = \frac{HLM - HLM1}{\max(HL, HM)},$$

where X_{lm} – components of the normalized symmetrical GLCM, L – dynamic range of gray scale image, μ – mean formulated as follows:

$$\mu_1 = \sum_{l,m=0}^{M-1} lm(X_{lm}),$$

$$\mu_l = \sum_{l,m=0}^{M-1} l(X_{lm}),$$

$$\mu_m = \sum_{l,m=0}^{M-1} m(X_{lm}),$$

$$HLM = -\sum_{l,m=0}^{M-1} X_{lm} \log(X_{lm}),$$

σ^2 denotes the variance level formulated as follows:

$$\sigma^2 = \sum_{l,m=0}^{M-1} X_{lm}(l-\mu)^2,$$

$$\sigma_l = \sum_{l,m=0}^{M-1} (l-\mu_1)^2 X_{lm},$$

$$\sigma_m = \sum_{l,m=0}^{M-1} (m-\mu_m)^2 X_{lm},$$

$$C_{lm} = \sum_{l,m=0}^{M-1} \frac{X_{lm}}{\sum X_{lm}},$$

$$A = \sum_{l,m=0}^{M-1} \frac{(l+m-2\mu\mu^3)X_{lm})}{\sigma^3(\sqrt{2(l+c)})^3},$$

$$B = \sum_{l,m=0}^{M-1} \frac{(l+m-2\mu\mu^4)X_{lm})}{4\sigma^4(l+c)^2},$$

C denotes the correlation measure.

3.2. Color gradient model

The color gradients of each pixel from all primary channels (R, G and B) are computed to measure the spatial variations of the region of interest. Here both X and Y coordinates are used to find the orientation of plant leaf edges in accordance with its position, which can explore the object types more appropriately. The computation of gradient vectors for formulating the background model offers optimal ways to discriminate the foreground and background regions of each incoming frame, as shown in Figs. 4 and 5. The nonlinear variations at the input frame sequence significantly influence the intensity values at each color channel but give less impact over gradient vectors, which include both magnitude and directions as shown below:

$$\Delta M = F(\Delta R_i, \Delta G_i, \Delta B_i),$$

where $i \in (1, n)$, where n is a number of coordinates. Here $(x,\ y)$ coordinates are used for gradient. The estimated resultant magnitude of final gradient ΔM at each coordinate $(x,\ y)$:

$$\Delta M(x, y) = \sqrt{\Delta {R_1}^2 + \Delta {R_2}^2 + \Delta {G_1}^2 + \Delta {G_2}^2 + \Delta {B_1}^2 + \Delta {B_2}^2}.$$

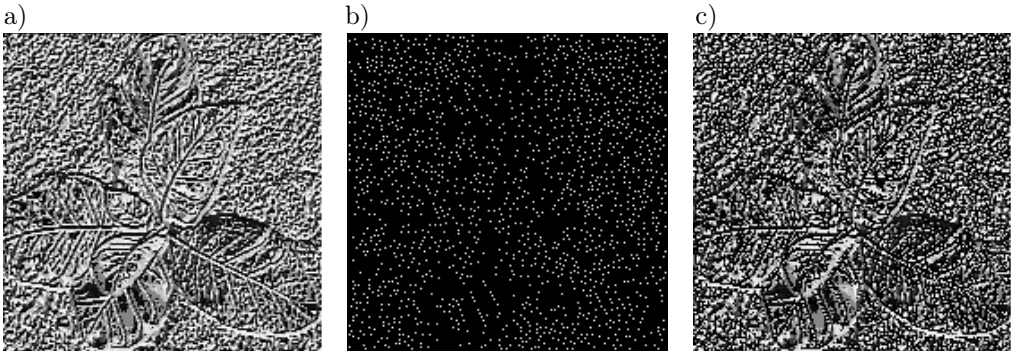

Fig. 4. Texture classification used for background modeling: a) LBP output, b) rotational invariant texture, c) uniform texture.

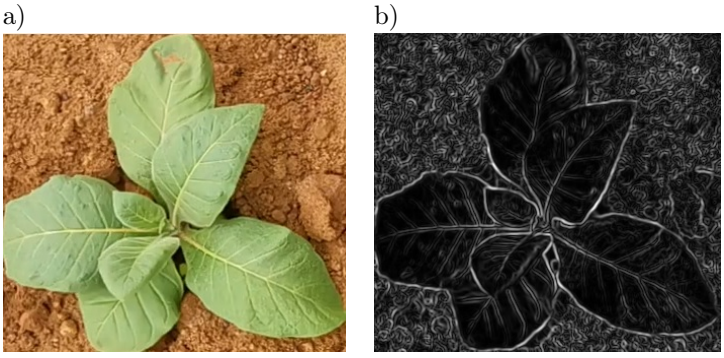

Fig. 5. Color gradient output: a) input plant, b) color gradient.

4. Review of experimental results

This FD method is tested over outdoor plant videos and various measures are evaluated to validate the performance metrics. The video dataset is collected from tobacco plantation site and various parameters of video dataset are as shown in Table 2. The performance validation considers tobacco videos of various environment conditions and the end results are compared with another classification model in order to show the superior detection rate and associated background suppression levels across different types of the video datasets. The

Table 2. Video parameters considered for performance validation.

Model	Parameters
The total number of videos tested	24
Video category	Set1: High-density plant rate Set2: Poorly illuminated condition
Video type	AVI format
Frame size Number of GLCM feature attributes used Color attributes used	320×240 20 3

performance comparison includes measures such as detection recall, precision, F-score and accuracy. A comparison is made accordingly.

4.1. Analysis of precision adjustments

To validate the performance of the tobacco plant disease identification and classification system, the results of FD are compared to find the best effective multimodal feature attribute-based BS method and to prove the robustness of the proposed model over BS using statistically independent gradient values with finite spatial information. The classification end results prove that the proposed hybrid texture-color gradient model shows improved detection accuracy in BS rate over the existing method. The detailed analysis and end results are shown in Table 3. The performance metrics of the proposed hierarchical spatial domain analysis for tobacco disease identification are also compared with the state-of-the-art spectral-domain disease identification model introduced by Gu *et al.* [12]. Due to a detailed exploration of texture abnormalities, the proposed texture-bound analysis model outperforms the existing method introduced by Gu *et al.* with improved classification accuracy, as shown in Table 4.

Table 3. Performance measures of the proposed FD system.

Measures	Image sets	
	Set1: High-density plant rate	Set2: Poorly illuminated videos
Recall	0.9722	0.9213
Precision	0.9548	0.3939
F-measure	0.8408	0.9118
Accuracy	0.9549	0.9131

Table 4. Comparative analysis with another state-of-art model.

Method used	Accuracy [%]
Spectral-domain analysis with wavelength selection model (Gu *et al.* [12])	85.20
Proposed spatial domain analysis	91.31

5. Conclusion

In this paper, we have explored the efficiency of hybrid texture and color gradient for a dynamic BS system. Statistical texture and color gradients were combined to identify the background and subtract it from foreground regions. This method was examined on several tobacco plant videos with dynamic background variation and real-time outdoor fields, and the performance validation in terms of detection accuracy and its consistency toward different nonlinear video dynamics confirms the robustness of the proposed plant detection system. The incorporation of multimodal feature attributes during template modeling comprising uniform and rotational invariant textures and color gradients, showed that an optimal background model can ensure dynamic BS efficiently with improved robustness and reliability.

References

1. N. Friedman, S. Russell, Image segmentation in video sequences: A probabilistic approach, [in:] *UAI'97: Proceedings of the Thirteenth conference on Uncertainty in artificial intelligence*, pp. 175–181, 1997.

2. A. Elgammal, D. Harwood, L.S. Davis, Non-parametric model for background subtraction, [in:] D. Vernon [Ed.], *Computer Vision – ECCV 2000. Lecture Notes in Computer Science*, Vol. 1843, pp. 751–767, Springer, Berlin, Heidelberg, 2000, doi: 10.1007/3-540-45053-X_48.

3. W. Wang, J. Yang, W. Gao, Modeling background and segmenting moving objects from compressed video, *IEEE Transactions on Circuits and Systems for Video Technology*, **18**(5): 670–681, 2008, doi: 10.1109/TCSVT.2008.918800.

4. T. Wang, Z. Zhu, Real time moving vehicle detection and reconstruction for improving classification, [in:] *2012 IEEE Workshop on the Applications of Computer Vision (WACV)*, 2012, pp. 497–502, doi: 10.1109/WACV.2012.6163039.

5. Z. Guo, L. Zhang, D. Zhang, A completed modeling of local binary pattern operator for texture classification, *IEEE Transactions on Image Processing*, **19**(6): 1657–1663, 2010, doi: 10.1109/TIP.2010.2044957.

6. D.Y. Lee, J.K. Ahn, C.C. Kim, Fast background subtraction algorithm using two-level sampling and silhouette detection, [in:] *2009 16th IEEE International Conference on Image Processing*, pp. 3177–3180, 2009, doi: 10.1109/icip.2009.5414397.

7. W. Zhou, Y. Liu, W. Zhang, L. Zhuang, N. Yu, Dynamic background subtraction using spatial-color binary patterns, [in:] *2011 Sixth International Conference on Image and Graphics*, pp. 314–319, 2011, doi: 10.1109/icig.2011.76.

8. J. Hu, T. Su, S. Jeng, Robust background subtraction with shadow and highlight removal for indoor surveillance, [in:] *2006 IEEE/RSJ International Conference on Intelligent Robots and Systems*, pp. 4545–4550, 2006, doi: 10.1109/IROS.2006.282156.

9. S. Liao, G. Zhao, V. Kellokumpu, M. Pietikäinen, S.Z. Li, Modeling pixel process with scale invariant local patterns for background subtraction in complex scenes, [in:] *2010 IEEE*

Computer Society Conference on Computer Vision and Pattern Recognition, pp. 1301–1306, 2010, doi: 10.1109/cvpr.2010.5539817.

10. A.D. Andrushia, A.T. Patricia, Artificial bee colony optimization (ABC) for grape leaves disease detection, *Evolving Systems*, **11**(1): 105–117, 2020, doi: 10.1007/s12530-019-09289-2.

11. S.K. Pravin Kumar, M.G. Sumithra, N. Saranya, Artificial bee colony-based fuzzy c means (ABC-FCM) segmentation algorithm and dimensionality reduction for leaf disease detection in bioinformatics, *The Journal of Supercomputing*, **75**(12): 8293–8311, 2019, doi: 10.1007/s11227-019-02999-z.

12. Q. Gu *et al.*, Early detection of tomato spotted wilt virus infection in tobacco using the hyperspectral imaging technique and machine learning algorithms, *Computers and Electronics in Agriculture*, **167**: 105066, 2019, doi: 10.1016/j.compag.2019.105066.

13. S.-Y. Chiu, C.-C. Chiu, S.S.-D. Xu, A background subtraction algorithm in complex environments based on category entropy analysis, *MDPI Applied Sciences*, **8**(6): Article ID 885, 2018, doi: 10.3390/app8060885.

14. X. Li, G. Li, Q. Jiang, Dynamic background subtraction method based on spatio-temporal classification, *IET Computer Vision*, **12**(4): 492–501, 2018, doi: 10.1049/iet-cvi.2017.0339.

15. Y. Yang, Q. Zhang, P. Wang, X. Hu, N. Wu, Moving object detection for dynamic background scenes based on spatiotemporal model, *Hindawi Advances in Multimedia*, **2017**: Article ID 5179013, 2017, doi: 10.1155/2017/5179013.

16. D. Sirohi, N. Kumar, P.S. Rana, Convolutional neural networks for 5G-enabled intelligent transportation system: A systematic review, *Computer Communications*, **153**: 459–498, 2020, doi: 10.1016/j.comcom.2020.01.058.

17. G.Y. Kim, R. Kim, S. Kim, K.D. Nam, S.U. Rha, J.H. Yoon, DNN inference offloading for object detection in 5G multi-access edge computing, [in:] *2021 International Conference on Information and Communication Technology Convergence*, pp. 389–392, 2021, doi: 10.1109/ictc52510.2021.9620821.

18. H. Li *et al.*, Human detection via image denoising for 5G-enabled intelligent applications, *Hindawi Wireless Communications and Mobile Computing*, **2021**: Article ID 5344890, 2021, doi: 10.1155/2021/5344890.

19. L. Nkenyereye, J. Kwon, Y.-H. Choi, Secure and lightweight cloud-assisted video reporting protocol over 5G-enabled vehicular networks, *MDPI Sensors*, **17**(10): 2191, 2017, doi: 10.3390/s17102191.

20. C. Kim, J. Lee, T. Han, Y.M. Kim, A hybrid framework combining background subtraction and deep neural networks for rapid person detection, *Journal of Big Data*, **5**(1): 1–24, 2018, doi: 10.1186/s40537-018-0131-x.

Received January 4, 2022; revised version March 8, 2022;
accepted May 14, 2022.